Sensors and Actuators A 271 (2018) 409–417

Contents lists available at ScienceDirect

Sensors and Actuators A: Physical

journal homepage: www.elsevier.com/locate/sna

Single ended capacitive self-sensing system for comb drives driven *XY* nanopositioners

Pablo G. del Corro[a,b,*], Matthias Imboden[c], Diego J. Pérez[d], David J. Bishop[d,e,f], Hernán Pastoriza[a,b,**]

[a] Laboratorio de Bajas Temperaturas, Instituto Balseiro, Centro Atómico Bariloche, Comisión Nacional de Energia Atómica, Av. Bustillo 9500, R8402AGP S. C. de Bariloche, Argentina
[b] Consejo Nacional de Investigaciones Científicas y Técnicas, Av. Rivadavia 1917, C1033AAJ C.A.B.A., Argentina
[c] Microsystems for Space Technologies Laboratory, École Polytechnique Fédérale de Lausanne (EPFL), Neuchâtel 2002, Switzerland
[d] Division of Material Science Boston University, Boston, MA 02215, United States
[e] Department of Physics, Boston University, Boston, MA 02215, United States
[f] Department of Electrical & Computer Engineering, Boston University, Boston, MA 02215, United States

ARTICLE INFO

Article history:
Received 24 July 2017
Received in revised form 7 November 2017
Accepted 8 November 2017
Available online 22 November 2017

Keywords:
Comb drives
Nanopositioners
Capacitive detection

ABSTRACT

This paper presents the implementation of a system to capacitively self-sense the position of a comb drive based MEMS *XY* nanopositioner from a single common node. The nanopositioner was fabricated using the multi-users PolyMUMPs process, on which comb capacitors fringe fields are large and out of plane forces cause considerable deflection. An extensive analysis of the comb-drive capacitance including the levitation effects and its correlation to the measurements is presented. Each axis is independently measured using frequency division multiplexing (FDM) techniques. Taking advantage of the symmetry of the nanopositioner itself, the sensitivity is doubled while eliminating the intrinsic capacitance of the device. The electrical measured noise is 2.5 aF/$\sqrt{\text{Hz}}$, for a sensing voltage $V_{sen} = 3V_{rms}$ and $f_{sen} = 150$ kHz, which is equivalent to 1.1 nm/$\sqrt{\text{Hz}}$ lateral displacement noise. This scheme can also be extended to N-degree of freedom nanopositioners.

© 2017 Elsevier B.V. All rights reserved.

1. Introduction

MEMS based nanopositioners have become very attractive for high precision nanopositioning systems such as STM [1], AFM [2], aligning of optical elements [3], nano-manipulation [4,5] and probe based high density data storage [6] because of their low power consumption, fast dynamic response and their possibility for large scale fabrication.

There are two commonly used driving systems for MEMS nanopositioners [2]: electrostatic and electro-thermal. In both cases, displacement in the order of tens of microns can be achieved [7–9]. For electrostatic actuation comb drive devices are typically used. The advantages of this type of actuation are the very low power consumption (in the order of μW) and fast dynamic response that can be achieved with them. On the other hand, electrothermal actuators (V-beam actuators, also called Chevron-type actuators; and hot arm thermal actuators) can generate significantly more force at low actuation voltages with the cost of significantly higher power consumption (in the order of mW).

A comb drive device can be represented electrically as a variable capacitor and electromechanically they can be used as actuator or as sensors. For nanopositioning, it is typical to use two comb drives mechanically and electrically connected where one generates the mechanical displacement, while the other one sense the displacement [7,10,11]. However, it has been demonstrated that comb drive devices can work as actuators for nanopositioning while simultaneously sensing its own displacement [12,13].

In general, for the capacitive read-out circuit differential configuration is used to reduce common-mode noise and parasitic effects. Also, for multi-electrode capacitive system, techniques such as frequency division multiplexing (FDM) or time division multiplexing (TDM) can be used to sense each differential output. On the one hand, TDM is attractive because allows to implement the read-out

* Corresponding author at: Laboratorio de Bajas Temperaturas, Instituto Balseiro, Centro Atómico Bariloche, Comisión Nacional de Energia Atómica, Av. Bustillo 9500, R8402AGP S. C. de Bariloche, Argentina.
** Principal corresponding author at: Laboratorio de Bajas Temperaturas, Instituto Balseiro, Centro Atómico Bariloche, Comisión Nacional de Energia Atómica, Av. Bustillo 9500, R8402AGP S. C. de Bariloche, Argentina.
E-mail addresses: pablodelcorro@cab.cnea.gov.ar (P.G. del Corro), hpastoriza@cab.cnea.gov.ar (H. Pastoriza).

https://doi.org/10.1016/j.sna.2017.11.021
0924-4247/© 2017 Elsevier B.V. All rights reserved.

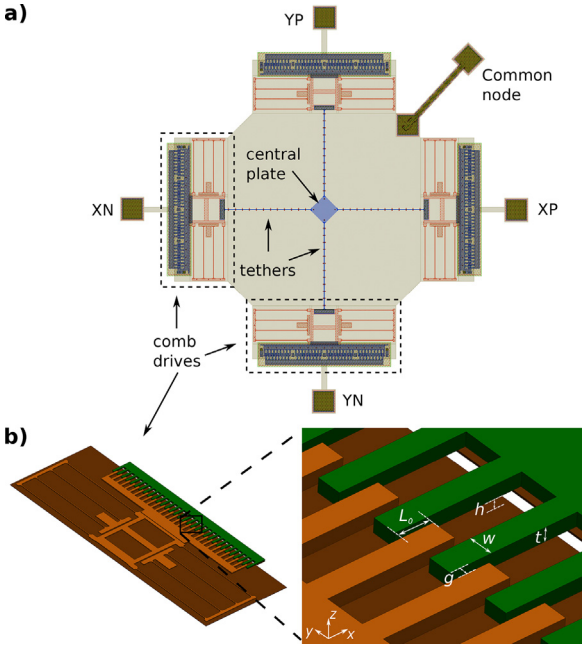

Fig. 1. (a) MEMS comb drive actuated nanopositioner. The central plate can be moved on the plane of the substrate actuated by the four comb drives connected to it through the tethers. (b) 3D representation of comb drive device. The zoom in the overlapped area of the combs shows its typical dimensions.

system using standard logic circuits [14], but has some limitations, e.g. excessive crosstalk, each sensor is measured sequentially, considerable increasing of noise due to the switching circuits. On the other hand, FDM can be implemented purely with analog circuits which can lead to better noise and crosstalk reduction and also allows parallel measurement of the array sensors [15].

In this paper, FDM technique is used to capacitively self-sense the displacement on a MEMS comb drive driven *XY* nanopositioners for both directions (*X* and *Y*) from a single common-node. A single readout circuit and a lock-in amplifier can be used to sense de displacement along either axis by simply switching the reference channel to the excitation frequency of the axis. This approach can be extrapolated to N-degrees of freedom.

A capacitance analysis for thin comb drive devices where, levitation and fringe field effect are considerable is performed to validate the experimental results. The discrepancy between experimental data and the model obtained is less than 2%. The measured capacitance noise is 2.5 aF/$\sqrt{\text{Hz}}$, for a sensing voltage $V_{sen} = 3V_{rms}$ and $f_{sen} = 150$ kHz. This result can be improved by increasing the sensing frequency up to 2 MHz which is the upper bandwidth limit of the circuit implemented.

2. Nanopositioner design

The device evaluated in this work was built using the PolyMUMPs multi-user process [16] provided by MEMSCAP. This process offers the possibility to design MEMS devices using three layers of highly doped poly-silicon and a single metal layer. The conductive substrate is isolated from the three layers by a 0.6 μm thick silicon nitride layer. The final gold layer is used to form high quality electrical connection to the MEMS.

The nanopositioner consists on a central plate suspended over the substrate by tethers that are mechanically and electrically connected to four identical comb drive actuators as shown in Fig. 1(a). The central plate can move in the plane of the substrate driven by the comb drive actuators. Opposite comb drives form a pull–pull type configuration to drive the central plate in one direction (e.g. *X* axis) and the additional set of comb drives move it in the orthogonal direction (e.g. *Y* axis). Each direction is divided in positive (P) and negative (N) respect to the initial condition of all four comb drives non-actuated (e.g. Y_P means the plate moving in *Y* direction towards the positive (P) way).

The spring constant of the tethers contribute about 10% of the spring constant in the transverse axis.

3. Comb drive actuator behavior

A comb drive is made up of two parts, an array of fixed fingers anchored to the substrate and another array of mobile interdigitated fingers suspended by springs. The fingers of width *w* and thickness *t* are separated by a gap *g* and overlapped by an initial length L_0 as is shown in Fig. 1(b). The comb drive behaves as an actuator when a bias voltage V_{act} (actuation voltage) is applied between the mobile and the fixed combs. The mobile structure is electrostatically attracted to the fixed comb and as result the overlap between the mobile and the fixed fingers L_0 increases to $L_0 + r$. Where *r* is the displacement intended to be use for nanopositioning proposes, referred to as *lateral displacement* and can be calculated as:

$$r = \frac{1}{2k_r}\frac{dC}{dr}V_{act}^2 = \delta_r V_{act}^2 \tag{1}$$

with k_r the spring constant in the *r* direction (which is a combination of the two folded flexural springs constants in *r* direction and the orthogonal tethers and flexural springs constants), *C* the total capacitance of the actuated comb drive and δ_r the lateral displacement electromechanical coupling coefficient.

Typically, in thin film comb drives (i.e. when $g \sim t$) as the fabricated using PolyMUMPs process, a grounding plane shorted electrically to the moving structure is placed underneath all the fingers to avoid unwanted charge accumulation in the substrate or a floating potential which could adversely affect the stability of the electromechanical response [17]. Secondary effects of having a grounded plane beneath the fingers are: (1) the reduction of the lateral displacement electromechanical coupling from δ_r to δ_r'; and (2) an asymmetry of the electric field in the overlapped mobile and fixed fingers area that induces a force normal to the plane of the substrate and causes to the mobile structure to levitate.

This out-of-plane/vertical displacement (levitation) can be calculated using the following equations [18]:

$$z = \frac{\delta_z\left(1 + \frac{r}{L_0}\right)V_{act}^2}{1 + \frac{\delta_z}{z_m}\left(1 + \frac{r}{L_0}\right)V_{act}^2} \tag{2}$$

with z_m the asymptotic value of levitation, δ_z the vertical electromechanical coupling coefficient and the factor $\left(1 + \frac{r}{L_0}\right)$ represents the contribution of lateral displacement to the levitation. Thus, levitation depends on lateral displacement. On the other hand, it can be demonstrated that lateral displacement is also levitation dependent (see appendix), then lateral displacement can be calculated as:

$$r = \delta_r'(1 + \theta z)V_{act}^2 \tag{3}$$

where δ_r' is the electromechanical coupling coefficient for a comb drive with grounded plane underneath the fingers, and θ a factor that computes the influence of levitation over lateral displacement.

If necessary, levitation can be reduced/controlled as described in Refs. [18–20] or by pulling all four combs simultaneously at a voltage higher than 30 V, that is the voltage needed to reach the maximum levitation.

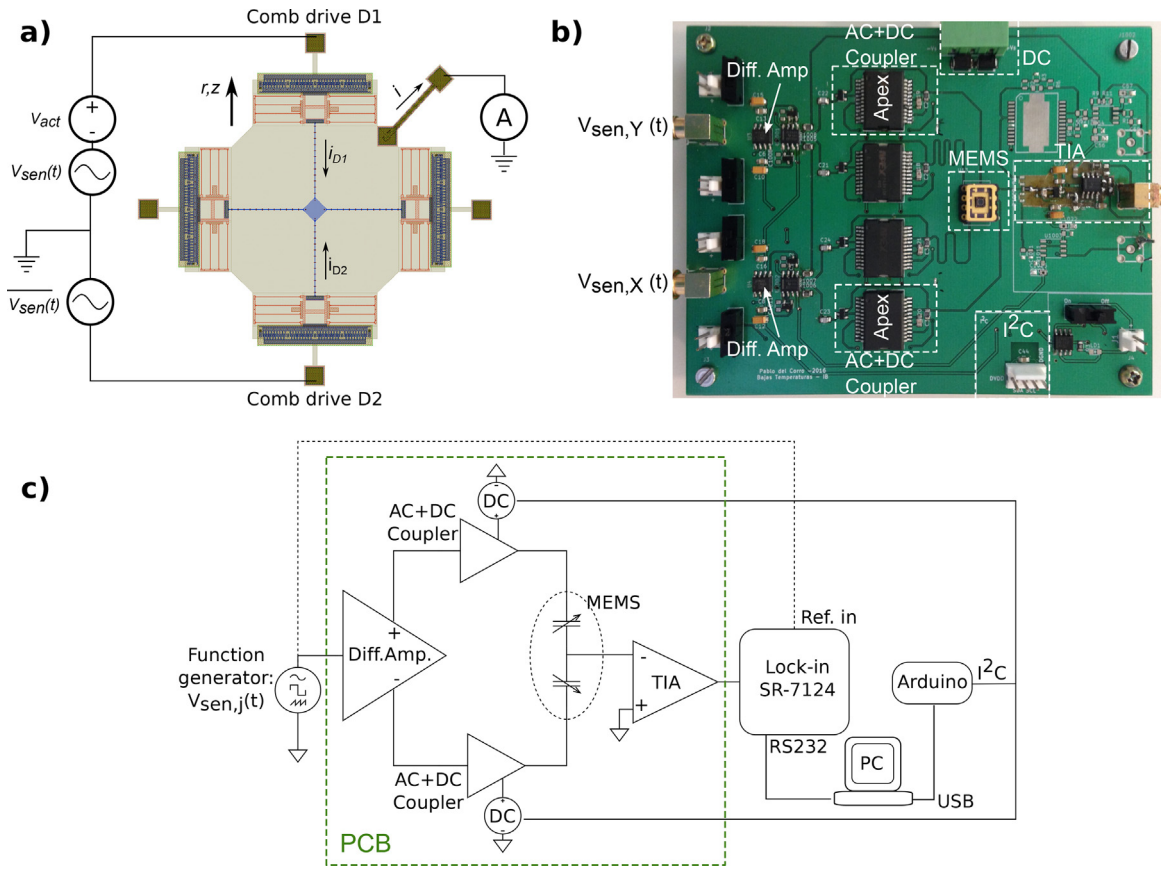

Fig. 2. (a) Electrical connection on one nanopositioner axis. By applying a balanced excitation signal, the device behaves electrically as capacitive bridge. The bias voltage causes the device to move. (b) Photo of the circuit fabricated. (c) Simplified diagram of the system implemented to sense and drive one axis of the nanopositioner. The dashed green rectangle indicates the stages of the system integrated on the PCB prototype. (For interpretation of the references to color in this figure legend, the reader is referred to the web version of this article.)

4. Simultaneous actuation and sensing scheme

4.1. Self-sensing concept

If a sinusoidal voltage source $V_{sen}(t) = V_{sen}\sin(2\pi f_{sen}t)$ (sensing voltage) is also added to actuation voltage V_{act}, a displacement current $i(t)$ will flow through the comb drive capacitor. Notice that, if V_{sen} and f_{sen} are fixed, and $f_{sen} \gg f_{res}$ with f_{res} the comb drive mechanical resonance frequency, the mechanical displacement due to the sensing signal can be negligible. As result, the contribution of the sensing voltage to the comb drive capacitance C can also be negligible [12], and the current $i_{comb}(t)$ will only be amplitude modulated by the changes C due to its mechanical displacement as a function of the bias voltage V_{act}.

$$\begin{aligned} i_{comb}(t) &= C(V_{act})\frac{dV_{sen}(t)}{dt} \\ &= 2\pi f_{sen}C(V_{act})V_{sen}\cos(2\pi f_{sen}t) \end{aligned} \tag{4}$$

This allow us to utilize the comb drive as an actuator for nanopositioning while simultaneously acting as a detector of its own displacement.

4.2. Balanced excitation capacitive bridge

Since all comb drives of our nanopositioner are identical to each other, each axis can be represented electrically as two identical variable capacitors with the mobile structures as common node. By applying a sensing voltage $V_{sen}(t) = V_{sen}\sin(2\pi f_{sen}t)$ to one axis comb, e.g. comb drive D1 in Fig. 2, and the same sensing voltage but with opposite phase ($\bar{V_{sen}}(t) = V_{sen}\sin(2\pi f_{sen}t + \pi)$) to the opposite comb of the same axis, the system forms a balanced excitation capacitive bridge [21] and any displacement can be detected as a change in the current $i(t)$ through the common node using an ammeter:

$$\begin{aligned} i(t) &= i_{D1}(t) + i_{D2}(t) \\ &= 2\pi f_{sen}\, V_{sen}\cos(2\pi f_{sen}t)(C_{D1} - C_{D2}) \\ &= 2\pi f_{sen}\, V_{sen}\cos(2\pi f_{sen}t)\Delta C \end{aligned} \tag{5}$$

where $i_{D1}(t)$ and $i_{D2}(t)$ are the currents trough the comb drive $D1$ and $D2$ respectively, and C_{D1} and C_{D2} are its capacitances.

The same bridge configuration can be applied to the orthogonal axis of the nanopositioner. By exciting the orthogonal axis with a frequency $f_{sen,j} \neq f_{sen,i}$ and $f_{sen,j} \gg f_{res,i}$, and using the adequate electronics, the displacement information on each axis can be independently demodulated.

4.3. Capacitance calculation

When applying an actuation voltage V_{act} to the comb drive D1, the mobile comb will displace laterally r and vertically z, producing a change on comb drive capacitance C_{D1} that can be expressed as the addition of the capacitance change due to the lateral displacement only plus the capacitance change due to the levitation only (see appendix):

$$C_{D1} = C_{D1_r} + C_{D1_z} = 2\delta_r' k_r\, r + \frac{2\delta_z k_z}{z_m}\left(z_m\, z - \frac{z^2}{2}\right) \tag{6}$$

Both comb drives of the axis are mechanically and electrically connected by the tethers to the central plate, so that the opposite comb drive displaces the same distance r but in this case moving in opposite direction relative to the fixed comb. Its been observed experimentally that the opposite comb drive is not influenced by levitation since this displacement is absorbed by the tethers. Thus, its capacitance C_{D2} can be obtained as:

$$C_{D2} = -C_{D2_r} = -2\delta_r' k_r r \tag{7}$$

From Eqs. (6) and (7), the capacitance of the bridge becomes:

$$\Delta C = C_{D1} - C_{D2} = C_{D1_r} + C_{D1_z} - (-C_{D2_r}) \tag{8}$$

$$= 4\delta_r' k_r r + \frac{2\delta_z k_z}{z_m}\left(z_m z - \frac{z^2}{2}\right)$$

Replacing r and z from Eqs. (3) and (2) respectively in Eq. (8):

$$\Delta C = 4k_r\delta_r'^2(1+\theta z)V_{act}^2 + \frac{2\delta_z k_z}{z_m} \cdot \left(\frac{\delta_z\left(1+\frac{r}{L_0}\right)V_{act}^2}{1+\frac{\delta_z}{z_m}\left(1+\frac{r}{L_0}\right)V_{act}^2} - \left(\frac{\frac{\delta_z}{4}\left(1+\frac{r}{L_0}\right)V_{act}^2}{1+\frac{\delta_z}{z_m}\left(1+\frac{r}{L_0}\right)V_{act}^2}\right)^2\right) \tag{9}$$

As can be seen, this is a recursive equation, with r and z dependent of each other. A first iteration results in a very good approximation (less than 2% deviation).

4.4. System implementation

Fig. 2(b) shows the PCB prototype built to drive and sense both axes of the nanopositioner. The diagram block of Fig. 2(c) shows a simplified schematic of the implemented system for one axis of the nanopositioner.

The balanced excitation signal needed for the bridge configuration is implemented using a LMH6551 differential amplifier. The differential amplifier specifies, as a characteristic of its differential output, the *output balance error*. Ideally, a output balance error of $-\infty$dB will mean that both outputs have the same amplitude and a phase difference of 180°. For the LMH6551, the typical output balance error is −70 dB (a factor ∼0.0003), this ensures a very good balanced excitation signal for our case. The LMH6551 is configured as single-ended input to differential output. The input of the differential amplifier is excited with a fixed AC sinusoidal voltage V_{sen} and frequency f_{sen} using a function generator. In common-mode, each output is the half of the voltage input (i.e. $V_{sen}/2$).

The DC actuation signal stage was designed to be controlled digitally using I^2C (e.g. with an *Arduino*) by controlling a digital to analog converter (DAC) DAC8574 integrated on the PCB prototype. The four DAC outputs (0–5 V range) are amplified 21 times using an Apex 341a high voltage amplifier, so that the actuation voltage can be controlled from 0 to 105 V (0–5 V × 21).

Typically the driven voltage for comb drive devices is within this range.

The *AC + DC coupler* stage has the function of coupling the sensing signal (AC voltage) with the DC actuation voltage. For this task, another Apex 341a is used, configured as an AC coupled inverting amplifier with the non-inverted input connected to the actuation voltage source through a low pass filter. The same configuration is replicated for the perpendicular axis of the nanopositioner.

The output current at the common node of the capacitive bridge is sensed using a low noise FET-input operational amplifier OPA657 configured as a trans-impedance amplifier (TIA). The amplifier has a 10 MHz bandwidth for a 200 kΩ trans-impedance gain. Thus, the trans-impedance amplifier output voltage $v(t)$ is:

$$v(t) = 200\ k\Omega\ i(t) \tag{10}$$

Finally, the trans-impedance amplifier voltage output is filtered and sensed using a lock-in amplifier SR-7124. The maximum operation frequency of this lock-in is 150 kHz. Thus, this is maximum frequency that can used to probe the bridge.

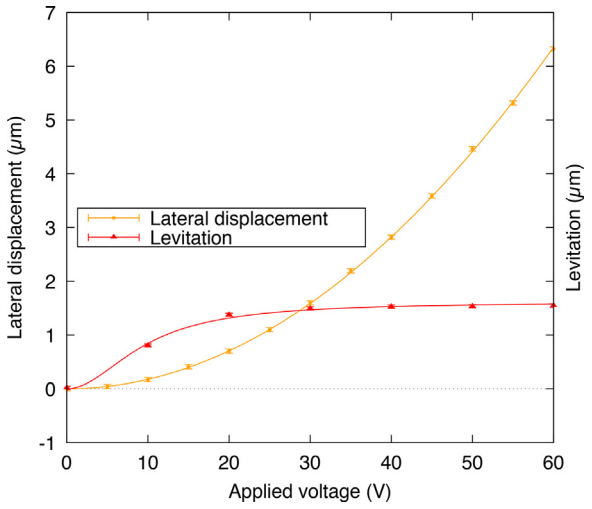

Fig. 3. Optical characterization of the nanopositioner response as a function of the actuation voltage V_{act}. Lateral displacement data is represented by orange dots and vertical displacement (levitation) by red dots. The lines are the fits using Eqs. (3) and (2). (For interpretation of the references to color in this figure legend, the reader is referred to the web version of this article.)

5. Experiments and results

5.1. Optical characterization

Lateral and vertical displacements were optically characterized for one comb drive of our nanopositioner, the results are shown in Fig. 3. The design dimensions for all comb drives are: $L_0 = 14\ \mu$m, $w = 6\ \mu$m, $t = 3.5\ \mu$m, $g = 2\ \mu$m, $N = 68$. Lateral displacement data is obtained using an optical microscope Nikon Eclipse L200N. Images of the combs overlap were taken after actuating the comb drive in voltage steps of 5 V and processed using a digital image correlation software (DIC) to determinate the lateral displacement with sub-pixel resolution. The uncertainty for this measurement is ±40 nm. Also, levitation was measured with a optical perfilometer with an uncertainty of ±10 nm.

The data for vertical and lateral displacement were fitted using Eqs. (2) and (3) respectively. The lateral displacement electromechanical coupling (δ_r') obtained from the fit is 1.77 nm/V^2, while the influence of levitation over lateral displacement θ is 0.04, thus θ can be despised. The measured vertical displacement electromechanical coupling (δ_z) is 17.6 nm/V^2 and the asymptotic value of levitation z_m is 1.59 μm. As all comb drives are identical to each other, these results can be extended to all of them.

5.2. Electrical characterization

In order to electrically characterize the nanopositioner response to the actuation voltage V_{act} (DC only), the setup shown in Fig. 2(c) was used. The sensing voltage applied to the Y axis was $V_{sen,Y} = 3V_{rms}$, at a frequency $f_{sen,Y}$ of 150 kHz. For the X axis, $V_{sen,X} = 3V_{rms}$ and $f_{sen,X}$ of 135 kHz. The lock-in output filter is set to a time constant (TC) of 10 ms and slope of 6 dB/octave for both

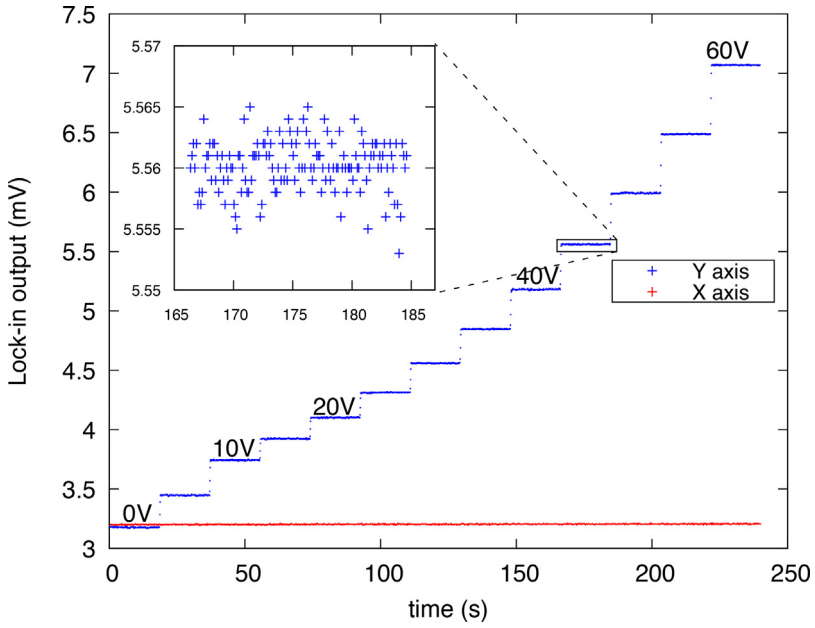

Fig. 4. Lock-in output over time while the actuation voltage V_{act} is sweep from 0 to 60 V in 5 V steps for the *Y* axis keeping *X* axis grounded. Each interval has 100 data points. The peak to peak noise is 10 μV, as it can be seen in the inset.

axis, which results in an equivalent noise bandwidth of about 25 Hz (1/(4TC)). Both axis were measured simultaneously by using the lock-in amplifier in *Dual Reference Mode*.

Fig. 4 shows the mechanical response of Y_P as a function of V_{act} measured at the output of the lock-in amplifier in 5 V steps form 0 to 60 V, while for *X* axis V_{act} was kept grounded (0 V). The inset shows a peak to peak noise of 10 μV or 3.53 μV_{rms}. The equivalent noise density is 0.7 $\mu V_{rms}/\sqrt{\text{Hz}}$. Notice that the lock-in output should be zero at V_{act} = 0 V but this is not the case as it can be observed in Fig. 4 (sensed voltage baseline at zero-actuation). This can be attributed to parasitic capacitances coupled at the trans-impedance amplifier input, which directly affect the sensitivity and the bandwidth of the detection system.

In our case, the bandwidth reduction is not critical since we are working at a relatively low frequency (150 kHz) while the roll-off frequency due to the parasitic capacitances is on the order of tens of MHz. Note that the bandwidth of the detection stage is defined by the bandwidth of the Apex-341a (about 2 MHz) used to couple the sensing and actuation signals. Regarding the sensitivity, it is very important to keep the input impedance of the trans-impedance amplifier as low as possible in order to reduce parasitic capacitances and the sensed voltage baseline at zero-actuation. The non

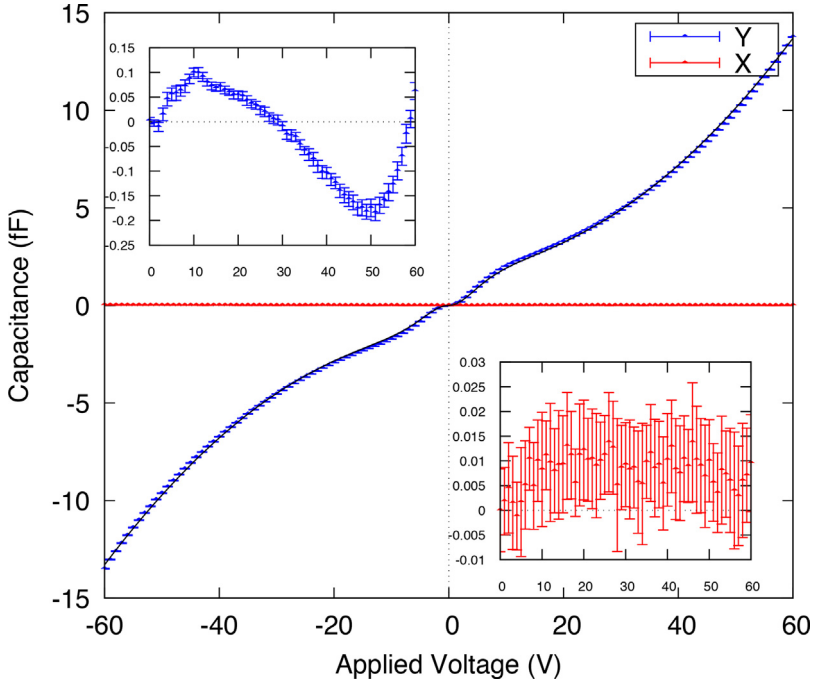

Fig. 5. Capacitance as function of the applied voltage V_{act}. For *Y* axis, V_{act} > 0 V, while for *X* axis, V_{act} = 0 V. Each data point is the mean value of 50 samples per V_{act} step of 1 V. The lines are fits using Eq. (9). The inset to the left is the deviation of Y_P from the fit. The inset to the right is a zoom in to X_P data.

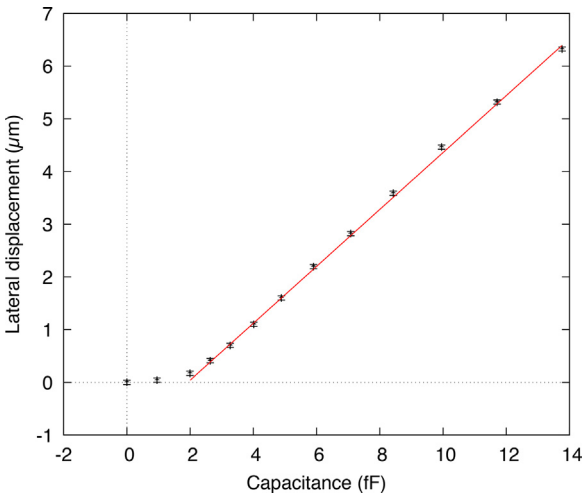

Fig. 6. Lateral displacement as a function of the capacitance.

zero baseline can be also caused by a poor output balance error at the differential amplifier output, mismatched components after differential output and capacitive coupling (crosstalk) between the nanopositioner common-node (sensing path) and the applied sensing signal V_{sen}.

The value obtained at the lock-in output can be converted to a capacitance value using Eqs. (5), (9) and (10). Fig. 5 shows the mechanical response of the *Y* axis while *X* is again kept to 0 V. In this case, positive (P) and negative (N) values are plotted. Each data point is the mean value of 50 samples (using the same TC and filter slope mentioned above) per V_{act} step of 1 V. The error was calculated as the standard deviation on each voltage step. The capacitance peak to peak error obtained was 35 aF or 2.5 aF/$\sqrt{\text{Hz}}$ capacitance equivalent noise density.

On the one hand, the inset on the bottom right side of Fig. 5 shows non variation in the signal detected on *X* while the applied voltage varies on the opposite axis. This can be translated as non-mechanical coupling between axes. On the other hand, the inset on the top left side, is the deviation of *Y* axis mechanical response to the actuation voltage respect to the fitted function using Eq. (9). The measured deviation is less than 2% over 60 V which is equivalent to about 90 nm. The deviation observed can be attributed to second order effects not considered in the approximation of Eq. (9).

The desired relation of the nanopositioner is lateral displacement vs capacitance. This correlation can be calibrated by measuring the deflection optically and plotting the results vs the measured capacitance. The results are depicted in Fig. 6. As can be seen, levitation produces a non linear relationship between lateral displacement and capacitance variation on the comb drive, but as the actuation voltage increases, levitation vanishes and this relationship becomes linear with a slope of 0.55 nm/aF. The absolute measurement error to determine lateral displacement is given by calibration certainty of the optical measurement (±40 nm). The error associated to the linear fit is about ±60 nm. While the noise detected at the output of the lock-in is about 20 nm peak to peak (±10 nm) or 1.1 nm/$\sqrt{\text{Hz}}$.

From Eq. (4) it can be seen that the current $i(t)$ sensed at the output of the capacitive bridge can be increased by increasing the sensing voltage amplitude V_{sen} or frequency f_{sen}. In our case, V_{sen} cannot further be increased ($3V_{rms}$ is the maximum voltage allowed at the input of the differential amplifier), but f_{sen} can be incremented over a factor 10 since the bandwidth of the circuit is about 2 MHz. Increasing $i(t)$ will result in a better signal to noise relationship, reducing the noise at the lock-in amplifier output.

5.3. Lateral displacement mechanical resonance

The measured bandwidth of the PCB prototype is about 1.97 MHz (from 30 kHz to 2 MHz) and the measured step response is 25 μs settling time with 15% overshoot. In order to compare the PCB prototype step response with nanopositioner mechanical step response, the lateral displacement mechanical resonance of one axis of the nanopositioner was measured. The results can be seen in Fig. 7.

The nanopositioner was connected to the circuit prototype and hooked up as shown in Fig. 2(c). The sensing voltage applied to the axis was V_{sen}= $3V_{rms}$, at a frequency f_{sen} of 150 kHz generated internally by the lock-in. Instead of a pure DC actuation voltage, V_{act} was configured with 40 V bias voltage and $1.5V_{rms}$ sine wave amplitude, and its frequency was sweep from 1 to 6 kHz in 20 Hz steps. The lock-in amplifier was configured in Tandem Mode. This mode perform two demodulations in series. The output filter of the first demodulator is configured with a low time constant (10 μs) in order to filter the excitation signal of 150 kHz without affecting

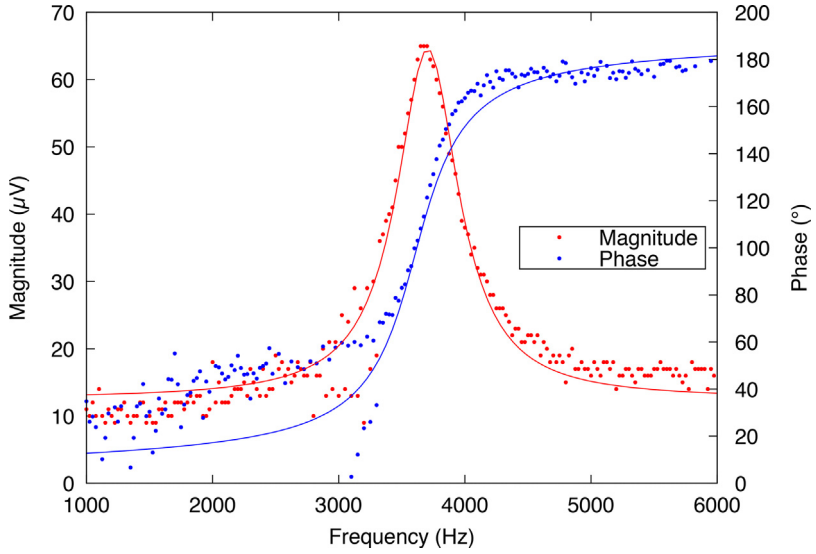

Fig. 7. Magnitude and phase vs frequency of the electrically measured lateral displacement mechanical resonance.

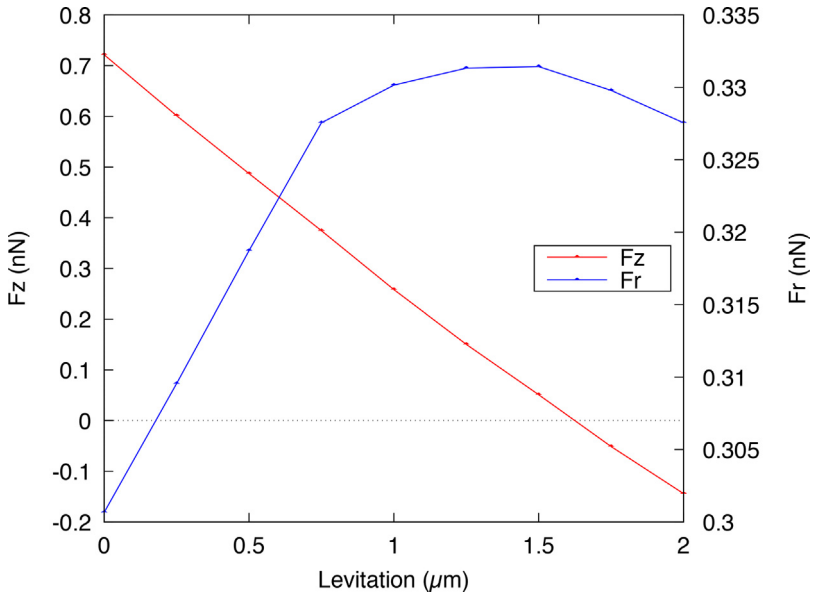

Fig. 8. FEA simulation of a comb drive electrostatic force over the mobile structure in r and z direction for a applied voltage of 1 V.

the low frequency signal amplitude. The second demodulator is locked-in to the V_{act} sine wave signal and configured with a 50 ms time constant output filter.

The mechanical resonance frequency obtained is 3.704 kHz measured at standard conditions of pressure and temperature. Similar results have been reached by using a high speed camera to optically measure the mechanical response of a single comb drive to a impulse signal.

By converting the mechanical resonance frequency obtained to a time scale, the device settling time is about 270 μs, which means that the circuit prototype settling time is 10 times faster than the nanopositioner mechanical response. The relative speed of the self-sensing and the mechanical response means that this method is suited for active feedback control. This can minimize the settling time [22]. Alternatively an accurate device characterization will also allow for efficient feed forward drive technique o be implemented [23].

6. Comparison with other capacitive position sensors

The capacitive sensitivity achieved with our setup (2.5 aF/$\sqrt{\text{Hz}}$) can be compared with other references. In Ref. [7] a 14 aF minimum standard deviation is reported for a bandwidth of 0.5 Hz using the same read out configuration (trans-impedance amplifier followed by a lock-in amplifier), while Ref. [10] obtained a 10 aF resolution (after 10000 samples average). A different approach for nanopositioning sensing is proposed in Ref. [13]: they use an LC circuit to detect changes in frequency as the comb drive capacitance changes, but not sensitivity is reported. Results of using commercial capacitance sensors are also reported in Refs. [24,11], 30 aF/$\sqrt{\text{Hz}}$ (using a AD7746 chip) and 4 aF/$\sqrt{\text{Hz}}$ (using a MS3110 chip) respectively.

While all these approaches lead to similar results as our implementation, Ref. [10] does not allow simultaneous actuation and detection (one comb drive is used for actuation and the other one for detection), and using commercial capacitance sensors or the approach proposed by [13] does not permit to sense multiple degree of freedom from a single sensor. Our method uniquely combines: (a) simultaneous actuation and detection, (b) low noise (2.5 aF/$\sqrt{\text{Hz}}$ or 1.1 nm/$\sqrt{\text{Hz}}$) and (c) the possibility of multi-electrode sensing from a single read-out circuit.

7. Conclusions

It has been shown that, with our MEMS nanopositioner design, it is possible to use the nanopositioner itself to obtain information of its own displacement and take advantage of its geometrical structure to implement a balanced excitation capacitive bridge. It has been demonstrated that the two axes displacement can be sensed independently from the same common node and sensing circuit. This configuration can be extended to N-axes excited at different frequencies. Optical and electrical characterization of the nanopositioner response to the actuation voltage have been carried out. Comb drive self-sense actuation and detection method have been combined with FDM techniques to implement the nanopositioner sense and drive system. The electrical measurement results have been discussed and compared to previous publications. The capacitance error obtained is 35 aF peak to peak or 2.5 aF/$\sqrt{\text{Hz}}$, for a sensing voltage $V_{sen} = 3V_{rms}$ and $f_{sen} = 150$ kHz. This result can be improved by increasing the sensing frequency up to 2 MHz which is the upper bandwidth limit of the circuit implemented.

Appendix A. Capacitive relation to in and out of plane forces

In this section, an analytic model of the comb drive capacitance variation as a function of V_{act} will be developed.

The total electrostatic force $\vec{F_E}$ over the mobile fingers in a comb drive is:

$$\vec{F_E} = \frac{1}{2}\vec{\nabla}CV_{act}^2; \quad \vec{\nabla}C = \left(\frac{\partial C}{\partial r}\hat{r}, \frac{\partial C}{\partial z}\hat{z}\right). \tag{11}$$

The force in the r and z directions can be calculated as [19,18]:

$$F_{Er} = \frac{1}{2}\frac{dC}{dr}V_{act}^2 = \alpha V_{act}^2, \tag{12}$$

$$F_{Ez} = \frac{1}{2}\frac{dC}{dz}V_{act}^2 = \beta\frac{z_m - z}{z_m}V_{act}^2.$$

where

$$\frac{dC}{dr} = 2\alpha, \quad \frac{dC}{dz} = 2\beta\frac{z_m - z}{z_m}. \tag{13}$$

The comb drive capacitance C is given by the line integral of the gradient $\vec{\nabla}C$:

$$C = \int_S \vec{\nabla}C(dr, dz) = \int_S \left(\frac{\partial C}{\partial r} d\hat{r}, \frac{\partial C}{\partial z} d\hat{z} \right) = \int_S \frac{\partial C}{\partial r} dr + \int_S \frac{\partial C}{\partial z} dz. \quad (14)$$

with S the curve that describes the comb drive displacement from the initial overlap between fingers to r and z values of lateral and vertical displacement respectively.

Combining (13) with (14):

$$\Rightarrow \Delta C = C - C_0 = 2\alpha r + \frac{2\beta}{z_m} \left(z_m z - \frac{z^2}{2} \right), \quad (15)$$

with C_0 the comb drive capacitance at zero actuation voltage (initial overlap between fingers) and ΔC the change of capacitance due to the comb drive displacement.

The electrostatic forces are balanced by the mechanical spring forces F_M as described by Hooke's law:

$$F_{Mr} = -k_r r, \quad F_{Mz} = -k_z z. \quad (16)$$

with k_r and k_z the comb drives spring constant in r and z directions respectively.

From (12) and (16), the lateral and vertical displacements can be determined as:

$$r = \frac{1}{2k_r} \frac{dC}{dr} V_{act}^2 = \frac{\alpha}{k_r} V_{act}^2 = \delta_r' V_{act}^2, \quad (17)$$

$$z = \frac{\frac{\beta}{k_z} V_{act}^2}{1 + \frac{\beta}{k_z z_m} V_{act}^2} = \frac{\delta_z V_{act}^2}{1 + \frac{\delta_z}{z_m} V_{act}^2},$$

with δ_r' the lateral displacement electromechanical coupling for a comb drive with a grounded plane underneath the fingers, z_m the asymptotic value of levitation, δ_z the vertical displacement electromechanical coupling.

By analyzing the force in lateral displacement direction over a mobile finger while this levitates, it can be shown that lateral displacement increases with levitation (see Fig. 8). This relationship can be then expressed as:

$$r' = \delta_r'(1 + \theta z') V_{act}^2, \quad (18)$$

with θ [m^{-1}] a factor that represents the influence of z' over the lateral displacement, where z' is the vertical displacement as a function of lateral displacement [18]:

$$z' = \frac{\delta_z \left(1 + \frac{r'}{L_0}\right) V_{act}^2}{1 + \frac{\delta_z}{z_m} \left(1 + \frac{r'}{L_0}\right) V_{act}^2}. \quad (19)$$

By combining (15), (18) and (19), the total capacitance can be written as:

$$\Delta C = 2\alpha r' + \frac{2\beta}{z_m} \left(z_m z' - \frac{z'^2}{2} \right). \quad (20)$$

This equation is recursive since r' and z' are dependent of each other. A very good approximation can be obtained (with a deviation smaller than 2%) by replacing r' and z' with r and z respectively after the first iteration:

$$\Delta C = 2\alpha\delta_r'(1 + \theta z) V_{act}^2 + \frac{2\beta}{z_m} \cdot \left(\frac{z_m \delta_z (1 + \frac{r}{L_0}) V_{act}^2}{1 + \frac{\delta_z}{z_m}(1 + \frac{r}{L_0}) V_{act}^2} - \left(\frac{\frac{\delta_z}{4}(1 + \frac{r}{L_0}) V_{act}^2}{1 + \frac{\delta_z}{z_m}(1 + \frac{r}{L_0}) V_{act}^2} \right)^2 \right). \quad (21)$$

References

[1] Y. Xu, N.C. MacDonald, S.A. Miller, Integrated micro-scanning tunneling microscope, Appl. Phys. Lett. 67 (1995) 2305, http://dx.doi.org/10.1063/1.115134.

[2] A.G. Fowler, A.N. Laskovski, A.C. Hammond, S.O.R. Moheimani, A 2-DOF electrostatically actuated MEMS nanopositioner for on-chip AFM, J. Microelectromech. Syst. 21 (4) (2012) 771–773, http://dx.doi.org/10.1109/JMEMS.2012.2191940.

[3] V. Aksyuk, D. Bishop, P. Gammel, Micromechanical xyz stage for use with optical elements, US Patent 5,963,367, October 5 1999.

[4] X. Liu, J. Tong, Y. Sun, A millimeter-sized nanomanipulator with sub-nanometer positioning resolution and large force output, Smart Mater. Struct. 16 (5) (2007) 1742 http://stacks.iop.org/0964-1726/16/i=5/a=029.

[5] D. Brouwer, B. de Jong, H. Soemers, Design and modeling of a six {DOFs} MEMS-based precision manipulator, Precis. Eng. 34 (2) (2010) 307–319, http://dx.doi.org/10.1016/j.precisioneng.2009.08.001 http://www.sciencedirect.com/science/article/pii/S0141635909001238.

[6] C.-H. Kim, H.-M. Jeong, J.-U. Jeon, Y.-K. Kim, Silicon micro XY-stage with a large area shuttle and no-etching holes for SPM-based data storage, J. Microelectromech. Syst. 12 (4) (2003) 470–478, http://dx.doi.org/10.1109/JMEMS.2003.809960.

[7] A.A. Kuijpers, R.J. Wiegerink, G.J.M. Krijnen, T.S.J. Lammerink, M. Elwenspoek, Capacitive long-range position sensor for microactuators, 17th IEEE International Conference on Micro Electro Mechanical Systems (MEMS), 2004 (2004) 544–547, http://dx.doi.org/10.1109/MEMS.2004.1290642.

[8] M. Imboden, H. Han, J. Chang, F. Pardo, C.A. Bolle, E. Lowell, D.J. Bishop, Atomic calligraphy: the direct writing of nanoscale structures using a microelectromechanical system, Nano Lett. 13 (7) (2013) 3379–3384, http://dx.doi.org/10.1021/nl401699w, pMID: 23782403.

[9] Y. Zhu, S.O.R. Moheimani, M.R. Yuce, A MEMS nanopositioner with thermal actuator and on-chip thermal sensor, 2010 IEEE Sensors (2010) 296–299, http://dx.doi.org/10.1109/ICSENS.2010.5689877.

[10] W.M. van Spengen, T.H. Oosterkamp, A sensitive electronic capacitance measurement system to measure the comb drive motion of surface micromachined MEMS devices, J. Micromech. Microeng. 17 (4) (2007) 828 http://stacks.iop.org/0960-1317/17/i=4/a=021.

[11] X. Zhang, B. Koo, S.M. Salapaka, J. Dong, P.M. Ferreira, Robust control of a MEMS probing device, IEEE/ASME Trans. Mechatron. 19 (1) (2014) 100–108, http://dx.doi.org/10.1109/TMECH.2012.2224122.

[12] J. Dong, P.M. Ferreira, Simultaneous actuation and displacement sensing for electrostatic drives, J. Micromech. Microeng. 18 (3) (2008) 035011 http://stacks.iop.org/0960-1317/18/i=3/a=035011.

[13] S.I. Moore, S.O.R. Moheimani, Displacement measurement with a self-sensing MEMS electrostatic drive, J. Microelectromech. Syst. 23 (3) (2014) 511–513, http://dx.doi.org/10.1109/JMEMS.2014.2314296.

[14] R. Brookhuis, T. Lammerink, R. Wiegerink, Differential capacitive sensing circuit for a multi-electrode capacitive force sensor, Sens. Actuators A: Phys. 234 (2015) 168–179, http://dx.doi.org/10.1016/j.sna.2015.08.020 http://www.sciencedirect.com/science/article/pii/S0924424715301126.

[15] A.M.K. Dagamseh, R.J. Wiegerink, T.S.J. Lammerink, G.J.M. Krijnen, Towards a high-resolution flow camera using artificial hair sensor arrays for flow pattern observations, Bioinspir. Biomim. 7 (4) (2012) 046009 http://stacks.iop.org/1748-3190/7/i=4/a=046009.

[16] A. Cowen, B. Hardy, R. Mahadevan, S. Wilcenski, PolyMUMPs Design Handbook, 1992 http://www.memscap.com/_data/assets/pdf_file/0019/1729/PolyMUMPs-DR-13-0.pdf.

[17] H.R. Shea, A. Gasparyan, H.B. Chan, S. Arney, R.E. Frahm, D. Lopez, S. Jin, R.P. McConnell, Effects of electrical leakage currents on MEMS reliability and performance, IEEE Trans. Device Mater. Reliab. 4 (2) (2004) 198–207, http://dx.doi.org/10.1109/TDMR.2004.826350.

[18] M. Imboden, J. Morrison, E. Lowell, H. Han, D.J. Bishop, Controlling levitation and enhancing displacement in electrostatic comb drives of MEMS actuators, J. Microelectromech. Syst. 23 (5) (2014) 1063–1072.

[19] W.C. Tang, M.G. Lim, R.T. Howe, Electrostatic comb drive levitation and control method, J. Microelectromech. Syst. 1 (4) (1992) 170–178.

[20] P.G. del Corro, M. Imboden, D.J. Bishop, H. Pastoriza, Comb drive designs with minimized levitation, J. Microelectromech. Syst. (99) (2016) 1–8, http://dx.doi.org/10.1109/JMEMS.2016.2614965.

[21] L.K. Baxter, Capacitive Sensors: Design and Applications, IEEE Press, 1997.

[22] S.I. Moore, S.O.R. Moheimani, Vibration control with mems electrostatic drives: a self-sensing approach, IEEE Trans. Control Syst. Technol. 23 (3) (2015) 1237–1244, http://dx.doi.org/10.1109/TCST.2014.1372363.

[23] M. Imboden, J. Chang, C. Pollock, E. Lowell, M. Akbulut, J. Morrison, T. Stark, T.G. Bifano, D.J. Bishop, High-speed control of electromechanical transduction: advanced drive techniques for optimized step-and-settle response of MEMS micromirrors, IEEE Control Syst. 36 (5) (2016) 48–76, http://dx.doi.org/10.1109/MCS.2016.2584338.

[24] X. Xi, T. Clancy, X. Wu, Y. Sun, X. Liu, A MEMS XY-stage integrating compliant mechanism for nanopositioning at sub-nanometer resolution, J. Micromech. Microeng. 26 (2) (2016) 025014 http://stacks.iop.org/0960-1317/26/i=2/a=025014.

Biographies

Pablo G. del Corro is an Electronic Engineer from National University of Santiago del Estero, Argentina. He obtained his Ph.D. diploma in Engineering Sciences at Instituto Balseiro, Argentina, in 2017. He thesis was focused on electrical signal detection and control circuits for MEMS sensor and actuators.

Matthias Imboden graduated from Bern University in 2004 with a Diploma (M.S.) in theoretical physics. He obtained his Ph.D. titled Diamond nano-electromechanical resonators: Dissipation and superconductivity, at Boston University in 2012. His research focuses on using micro and nano-electromechanical systems for both research and technology development. Topics of interest include nanoscale fabrication, quench condensed superconductivity, tunable plasmonics, smart lighting systems, and mechanobiology. Dr. Imboden is a member for American Physics Society and serves on the EuroEAP Outreach & Dissemination committee. He is currently working at EPFL, Switzerland as a Marie Sklodowska-Curie Fellow.

Diego J. Perez received a B.S. in Physics from the Universidad Nacional de San Luis in Argentina and a Ph.D. in Physics from the Instituto Balseiro, Universidad Nacional de Cuyo in Argentina. His Ph.D. research included developing and implementation of a high-sensitive micromechanical magnetometer to study phase transitions in superconducting vortex systems and in the design of MEMS devices used to measure small forces. He currently works as a post doctorate researcher in the Electrical & Computer Engineering Department at Boston University and as a CNST Visiting Fellow in the Nanofabrication Research Group at NIST. His work focuses on novel Casimir effect measurements in micro and nanoscale devices.

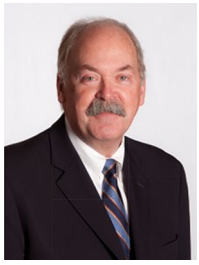

David J. Bishop became a member of the IEEE in 2011. He received his BS in Physics from Syracuse University in 1973 and his MS in Physics in 1977 and his Ph.D. in Physics in 1978, both from Cornell University. He is currently the Head of the Division of Materials Science and Engineering, Boston University and also a Professor of Physics and a Professor of Electrical Engineering. Previously he was the Chief Technology Officer (CTO) and Chief Operating Officer (COO) of LGS, the wholly-owned subsidiary of Alcatel-Lucent dedicated to serving theU.S. federal government market with advanced R&D solutions. Before joining LGS, Dr Bishop was the President of Government Research & Security Solutions for Bell Labs, Lucent Technologies. Dr. Bishop is a Bell Labs Fellow and in his previous positions with Lucent served as Nanotechnology Research VP for Bell Labs, Lucent Technologies; President of the New Jersey Nanotechnology Consortium and the Physical Sciences Research VP. He joined AT&T-Bell Laboratories Bell Labs in 1978 as a postdoctoral member of staff and in 1979 became a Member of the Technical Staff. In 1988 he was made a Distinguished Member of the Technical Staff and later that same year was promoted to Department Head, Bell Laboratories. Professor Bishop is a member and fellow of the American Physical Society, a member of the MRS and a recipient of the APS Pake Prize.

Hernán Pastoriza received his PhD degree in Physics from Instituto Balseiro in 1994 and has attended post doctoral positions in Leiden University and Neuchtel University. He is currently Principal Researcher in CONICET, Researcher in CNEA, and Professor in Instituto Balseiro. He has more than 50 publications in Condensed Matter Physics, Applied Physics and Microsensors. Since 2002 he has been involved in the development of microelectromechanical systems for superconductivity research, satellite sensors and biomedical sensors.